Phase Diagrams and Water Activities of Aqueous Dicarboxylic Acid Systems of Atmospheric Importance

Keith D. Beyer,* Katherine Friesen, Jameson R. Bothe, and Benjamin Palet

Department of Chemistry, University of Wisconsin−La Crosse, La Crosse, Wisconsin 54601

Received: July 07, 2008; Revised Manuscript Received: September 23, 2008

We have studied liquid/solid phase diagrams and water activities of the dicarboxylic acid/water binary systems for maleic, *dl*-malic, glutaric, and succinc acids using differential scanning calorimetry, infrared (IR) spectroscopy of thin films, and conductivity analysis of saturated solutions. For each binary system we report the measurements of the ice melting envelope, the acid dissolution envelope, and the ice/acid eutectic temperature and composition. Water activities have been determined by using the freezing point depression of ice. Additionally, an irreversible solid/solid phase transition for maleic acid was observed in both DSC and IR studies likely due to the conversion of a meta-stable crystal form of maleic acid to its most stable crystal form. In general we find good agreement with literature values for temperature-dependent acid solubilities.

Introduction

Recent field measurements have shown that a significant fraction of tropospheric aerosols in many regions is organic.[1−7] Studies have shown that the incorporation of organic compounds into ammonium sulfate aerosols changes their deliquescence, efflorescence, and hygroscopic properties, and potentially their crystallization properties.[8−12] The various physical properties of these systems have recently been summarized and modeled at 298.15 K.[13,14] This necessitates understanding the impact of organic substances on the phase transitions of aqueous systems that make up tropospheric aerosols at tropospheric temperatures. Some of the most abundant organic compounds found in aerosols are the dicarboxylic acids: oxalic, malonic, succinic, maleic, glutaric, and multifunctional acids such as malic[4,6] though both oxalic and succinic are of significantly lower solubility than the other acids. Very little is known about the thermodynamics of these systems in water at temperatures below 298 K. In particular, fundamental physical data are needed on these systems for incorporation into atmospheric models in order to better predict atmospheric cloud properties.[13,14] Data such as the equilibrium freezing temperature (solute saturation temperature) as a function of solute concentration are among the basic parameters that need to be experimentally determined. In this study we focus on the aqueous systems of maleic, *dl*-malic, glutaric, and succinic acids.

Experimental Section

Sample Preparation. Samples were prepared by dissolving 99%+ pure ACS reagent grade $C_4H_4O_4$ (maleic acid, F.W. 116.07 g/mol), $C_4H_6O_4$ (succinic acid, F.W. 118.09 g/mol), $C_4H_6O_5$ (*dl*-malic acid, F.W. 134.09 g/mol), or $C_5H_8O_4$ (glutaric acid, F.W. 132.11 g/mol), respectively, (all supplied by Aldrich) with Culligan purified water. Samples were made gravimetrically on a 0.1 mg balance with accuracy of ±0.2 mg.

Infrared Spectra. The sample cell used for infrared spectra is shown schematically and explained in detail in previous literature.[15] Briefly, a small drop of binary solution was placed between two ZnSe windows, which were held in the center of an aluminum block by a threaded metal ring. Sample volumes were approximately 2 μL. On each side of the aluminum block a Pyrex cell was purged with dry nitrogen gas. KBr windows were placed on the end of each cell, sealed with o-rings, and held in place by metal clamps. Heat tape was wrapped around the purge cells to prevent condensation on the KBr windows. The sample was cooled by pouring liquid nitrogen into a circular aluminum cup attached to the top of the main cell. The cell block was warmed by resistive heaters connected to a temperature controller. Temperature was measured by a copper/constantan thermocouple placed at the edge of the ZnSe windows and connected to the temperature controller. The temperature of the cell was calibrated using Culligan purified water and high-purity organic solvents (Aldrich): decane, octane, and acetic anhydride of which the melting points are 243.5, 216.4, and 200.2 K, respectively.[16] The IR cell temperatures are known on average to within ±1.3 K, i.e., a temperature we measured in the IR cell of a specific transition is within 1.3 K of the transition temperature we measure (of the same transition) using the DSC.

Spectra were obtained with a Bruker Tensor 37 FTIR with an MCT-B detector at 4 cm^{-1} resolution. Each spectrum was the average of 10 scans. Before spectra were taken of a sample, a background scan was obtained from a dry, purged sample cell. Samples were cooled to 183 K at 3 deg/min and then allowed to warm to room temperature without resistive heating, typically this was 1 deg/min. In some cases samples were heated above room temperature with resistive heating for this segment. Scans were taken every 10 deg on warming until the eutectic was approached and then scans were taken every degree and then every 0.2 deg.

Differential Scanning Calorimeter. Thermal data were obtained with both a Mettler Toledo DSC 822e with liquid nitrogen cooling and a Mettler Toledo DSC 822e cooled via an intracooler. Each DSC utilized an HSS7 sensor. Industrial grade nitrogen gas was used as a purge gas with a flow rate of 50 mL/min. The temperature reproducibility of these instruments is better than ± 0.05 K. Our accuracy is estimated to be ±0.9 K with a probability of 0.94 based on a four-point temperature

* Corresponding author. E-mail: beyer.keit@uwlax.edu.

10.1021/jp805985t CCC: $40.75
Published on Web 10/29/2008

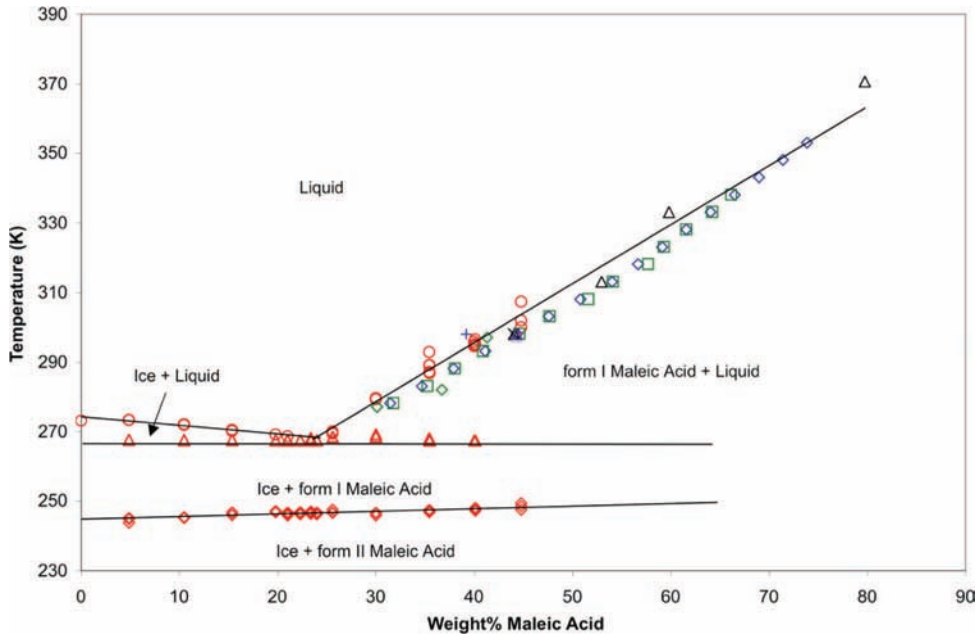

Figure 1. Phase diagram of the maleic acid/water binary system. Red points are our DSC data: circles, final ice melt or acid dissolution; triangles, eutectic melt; diamonds, solid/solid phase transition (see text). Literature data: black triangles, Weiss and Downs;[19] blue diamonds, Lange and Sinks;[20] green squares, Apelblat and Manzurola;[21] green diamonds, Brooks et al.;[10] blue plus, Wise et al.;[11]black ex, Marcolli et al.;[12] purple diamond, prediction of the E-AIM.[13,14]

calibration[17] using indium, HPLC grade water, anhydrous, high-purity (99%+) octane, and anhydrous, high-purity heptane (99%+) from Aldrich, the latter three stored under nitrogen. The sensitivity of our instrument to thermal signals has been determined to be on the order of <10 ppm by mass utilizing the HSS7 sensor.

Samples were contained in a 40 μL aluminum pan and typically had a mass of approximately 15 to 25 mg. Each sample was weighed before and after the experiment using a Mettler-Toledo AT20 microgram balance. The average mass loss from evaporation during the experiment was less than 1%. A typical sample was cooled to 183 K at 10 deg/min, held at that temperature for 5 min, and then warmed at a rate of 1 deg/min to a temperature at least 5 K above the predicted melting (or dissolution) point. Melting is an endothermic process and DSC instruments measure the difference in heat flow between a sample and a reference, thereby generating a thermogram showing this difference. For eutectic transitions, we record the onset temperature of the transition (first appearance of liquid), but for final melting of a phase we record the peak temperature, which represents the point just before the last solid melts or dissolves into solution. The exact point of existence of the last "solid" cluster is ill-defined, so it is common practice to utilize the peak temperature as the final melting/dissolution point.[18]

Conductivity. For systems that had weak thermal signals, thus making dissolution of the acid difficult to detect using DSC, we employed conductivity analysis using a Mettler-Toledo SevenMulti conductivity meter with temperature compensation. In these experiments a saturated solution was made and stirred continuously. Conductivity of the solution was measured as temperature was increased. Complete dissolution of the acid is indicated by a discontinuous change in the slope of the conductivity. These experiments were utilized for succinic, malic, and glutaric acid systems. A figure of a typical data set is given in Figure 1S in the Supporting Information (39.21 wt % glutaric acid/water solution).

TABLE 1: Polynomial Coefficients Corresponding to Eq 1 for the Ice Melting and Acid Dissolution Envelopes for Succinic, Maleic, Malic, and Glutaric Acids

	A_2	A_1	A_0	valid acid concn range (wt %)
ice		−0.2545	273.0	0−2.08
succinic acid	−0.166	6.151	260.4	2.08−15.5
ice		−0.2491	274.3	0−23.9
maleic acid		1.697	227.7	23.9−50
ice	−0.005571	−0.02060	273.0	0−42.4
malic acid		2.215	170.25	42.4−74
ice	−0.0145	0.0693	273.15	0−18.4
glutaric acid		0.7271	256.14	18.4−70

Results

Maleic Acid/Water ($C_4H_4O_4/H_2O$). ***Phase Diagram.*** Figure 1 shows the phase diagram for the maleic acid/water system. Included on the diagram are the DSC results and solubility data from the literature.[10−12,19−21] The raw experimental data for this system are included in Table 1S in the Supporting Information.The temperature data were parametrized using the following equation:

$$T = A_2X^2 + A_1X + A_0 \quad (1)$$

where T is the melting temperature (in Kelvin), X is the acid concentration (in wt %), and the A_i terms are the respective polynomial coefficients. To determine the eutectic composition and temperature, the equations were solved simultaneously. The polynomial coefficients for the fit of the ice and acid liquidus lines using eq 1 are given in Table 1. The DSC data for maleic acid has an average eutectic temperature of 267.78 ± 0.40 K, which is in good agreement with the value of 268.32 K at 23.9 wt % maleic acid calculated from the analysis of the ice melt and acid dissolution curves using eq 1 and the parameters in

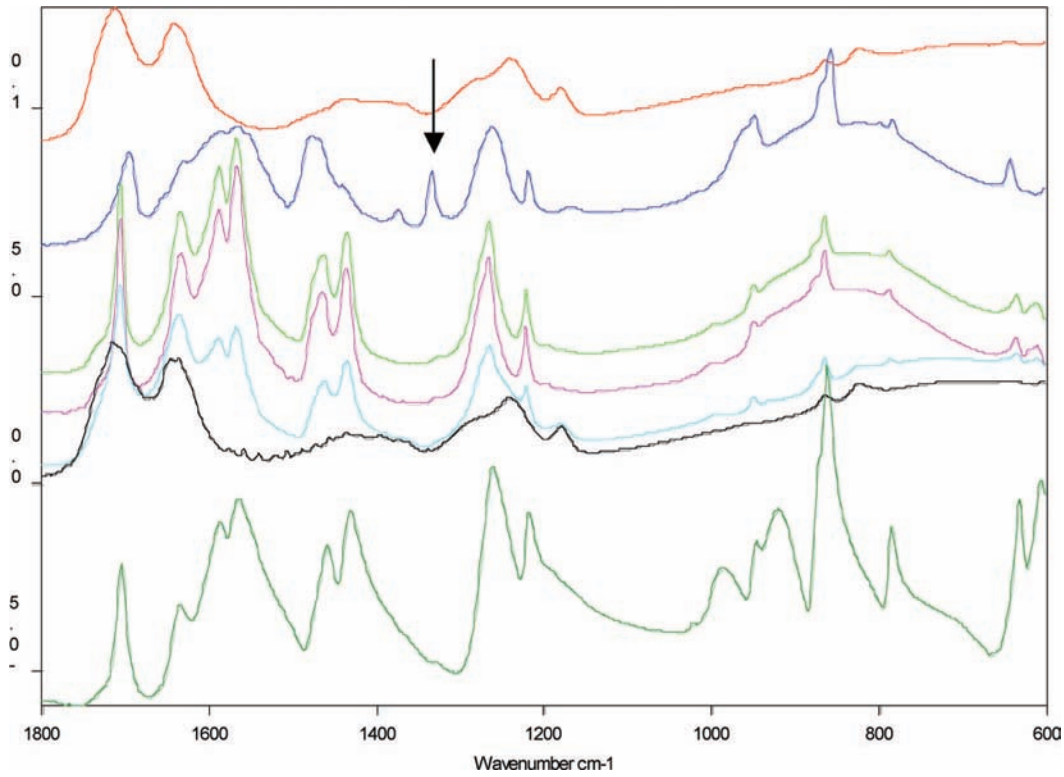

Figure 2. IR spectra of a 40.0 wt % maleic acid sample as a function of temperature. Spectra are as follows with offsets in parentheses: red (+1.0), 294.5 K, sample is completely liquid; blue (+0.75), 243.4 K, sample has completely frozen to ice and a meta-stable crystal form of maleic acid (arrow indicates position of peak at 1330 cm^{-1}); light green (+0.4), 262.7 K, after the sample has been cooled to 185 K, it is then warmed to 262.7 K, as can be seen the peak at 1330 cm^{-1} is gone along with other shifts in various peaks due to the conversion of the meta-stable crystal form to the most stable form of maleic acid (see text); purple (+0.3), 243.4 K, the sample was cooled again to 185 K and then warmed, no shift back to the meta-stable solid fingerprint is seen; light blue (+0.15), 267.4 K, ice has melted leaving signatures of maleic acid; black (+0.1), 294.5 K, maleic acid dissolves into solution leaving a spectrum identical to the original; dark green (−0.6, multiplied by 10), 298 K spectrum of pure solid maleic acid taken with an ATR accessory.

Table 1. In the DSC experiments at concentrations within about 3 wt % of the eutectic, the eutectic peak dominates the thermogram, obscuring any other smaller peaks in this region; therefore, the ice melt peak is not resolved around this point and the final melt data are not included in Figure 1.

In the DSC and IR experiments we observed an irreversible transition at approximately 247 K. The average transition temperature in the DSC experiments was 246.71 ± 0.96 K. The normalized energy of the transition increased linearly with maleic acid concentration, indicating the thermal transition is due to a crystal change involving maleic acid. In the IR experiments, we have detected significant changes to the fingerprint region at the temperature of this transition. As an example, Figure 2 shows the IR spectra for a 40.0 wt % maleic acid sample at various stages of a cooling, warming, cooling, warming experiment. We performed this type of experiment with both IR and DSC instruments to determine if the 247 K transition was reversible. The initial cooling/warming sequence was typical of all samples we studied. As the samples were cooled from room temperature to 183 K, the blue spectrum shown in Figure 2 appeared at 243−233 K: the temperature at which the samples initially froze completely. Samples were typically cooled to a low point of 185 K. Then, upon warming, significant peak shifts and changes in absorbance in the fingerprint region occurred between 246 and 250 K. A summary of the major changes is given in Table 2 along with the peaks observed in an infrared spectrum of solid maleic acid using an attenuated total reflectance (ATR) accessory at room temperature. Most notably, a peak at 1330 cm^{-1} disappears during this transition and will be discussed below in light of the conclusions of Brooks et al.[22] In the experiment represented in Figure 2, the sample was then recooled to 183 K and again allowed to warm to room temperature. In both the DSC and IR experiments the "maleic acid/ice" spectrum remained upon cooling to lower temperatures, and thus the transition was not observed on the second cooling/warming cycle, as seen in the IR spectra of Figure 2. This behavior is confirmed in the DSC experiment shown in Figure 3 where the same cooling−heating−cooling−heating program is used. We therefore conclude that the transition is likely a meta-stable maleic acid crystal structure (hereafter referred to as "form II") relaxing into a more stable form (hereafter referred to as "form I"), which is an irreversible change. From the cooling−heating−cooling−heating experiments we can conclude that form I is more stable at the temperatures of the experiment. It is unlikely there is a significant barrier to the formation of form II since it initially forms from the liquid. Thus the observation that form II does not crystallize from form I of maleic acid implies that form I is more stable at all temperatures, and thus implies forms I and II are monotropic.

Brooks et al.[22] have studied the maleic acid/ammonium sulfate system and its uptake of water, reporting two infrared spectra for maleic acid: one for "dry" aerosols (10% relative humidity) and another for a dry maleic acid sample deposited on a NaCl window. Our maleic acid form II/ice spectrum (blue spectrum in Figure 2) is essentially identical to the "dry" maleic acid aerosol spectrum of Brooks et al. in the 1800−1200 cm^{-1} range, while our maleic acid form I/ice spectrum (light green and magenta spectra of Figure 2) is identical to their dry maleic acid deposited on a NaCl window spectrum. Both of these latter

TABLE 2: IR Frequencies and Normalized Peak Intensities for a Frozen 40.0 wt % Maleic Acid/Water Film and Dry Maleic Acid in an ATR Accessory

meta-stable solid/ice film (form II)		maleic acid/ice film (form I)		dry maleic aicd ATR	
ν (cm^{-1})	normalized absorbance[a]	ν (cm^{-1})	normalized absorbance[a]	ν (cm^{-1})	normalized absorbance[b]
1695	0.38	1707	0.80	1705	0.58
1632	0.34	1634	0.67	1635	0.41
1588	0.47	1588	0.86	1587	0.77
1567	0.48	1567	1.00	1565	0.86
1478	0.45	1464	0.50	1459	0.67
1441	0.23	1436	0.59	1432	0.81
1375	0.14				
1335	0.30				
1263	0.48	1266	0.64	1261	1.00
1219	0.30	1222	0.48	1218	0.80

[a] Normalized values are absorbance + 0.11 (abs at 1772 cm^{-1} = −0.11) divided by largest absorbance. [b] Normalized values are absorbance − 0.000805 (abs at 1772 cm^{-1} = 0.000805) divided by largest absorbance.

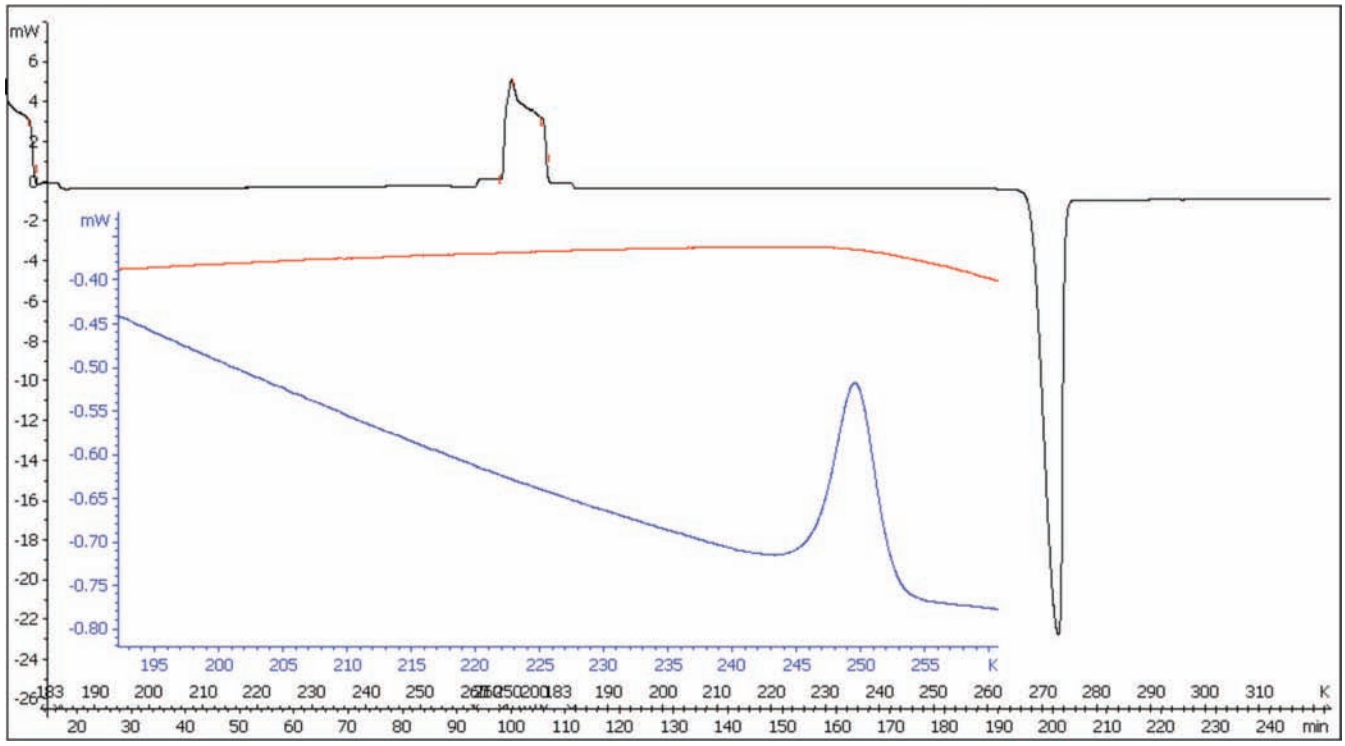

Figure 3. DSC thermogram of 40 wt % maleic acid/water sample. Black thermogram shows heating of the sample from 183 to 260 K, with the irreversible solid/solid phase transition occurring at 246 K. The increase in the baseline at 260 K is due to the change in heating from 1 deg/min to an isothermal segment. The large increase in the baseline that follows is due to the cooling at 10 deg/min to 183 K, followed by another isotherm at that temperature. Finally, the sample is heated from 183 to 298 K at 1 deg/min. The blue thermogram is an expansion of the second heating segment showing no signal due to the solid/solid phase transition from 183 to 267 K.

spectra match very well with our spectrum of dry maleic acid crystals taken with an ATR accessory in our laboratory (dark green spectrum of Figure 2). Brooks et al. explained their "dry" aerosol spectrum as being a mixture of two distinct structures of buthenedioic acid: maleic acid in the interior and fumaric acid at the surface of their particles. The structure of these two molecules is given in Figure 4. Brooks et al. report a spectrum for fumaric acid deposited on a NaCl window (see their Figure 3) and conclude that their "dry" aerosol spectrum is a mixture of maleic in the bulk and fumaric at the surface since their spectrum for fumaric acid does not match their "dry" aerosol spectrum, but does have a "shoulder" peak at 1330 cm^{-1}. However, this seems an implausible explanation for our spectrum for form II maleic acid (which is identical to the "dry" spectrum of Brooks et al.), since maleic and fumaric acids appear to be quite stable up to high temperatures (Brooks et al. performed their experiments at 273 K, and Macoas et al.[23]

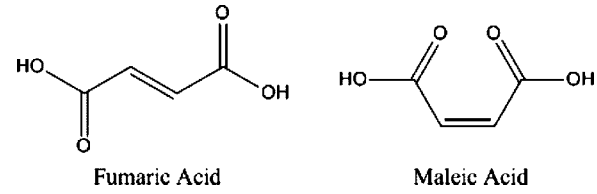

Figure 4. Structures of fumaric and maleic acids.

prepared samples of maleic and fumaric acids at temperatures of 353 and 408 K, respectively). Thus, the conversion of fumaric to maleic acids as the explanation for our transition at 247 K is highly unlikely. It is unclear why our form II maleic acid spectrum matches the "dry" aerosol spectrum of Brooks et al. in the 1800−1100 cm^{-1} region, which they conclude is a mixture of maleic and fumaric acids.

Macoas et al.[23] reported several measured and calculated IR specra for various conformers of maleic and fumaric acids in

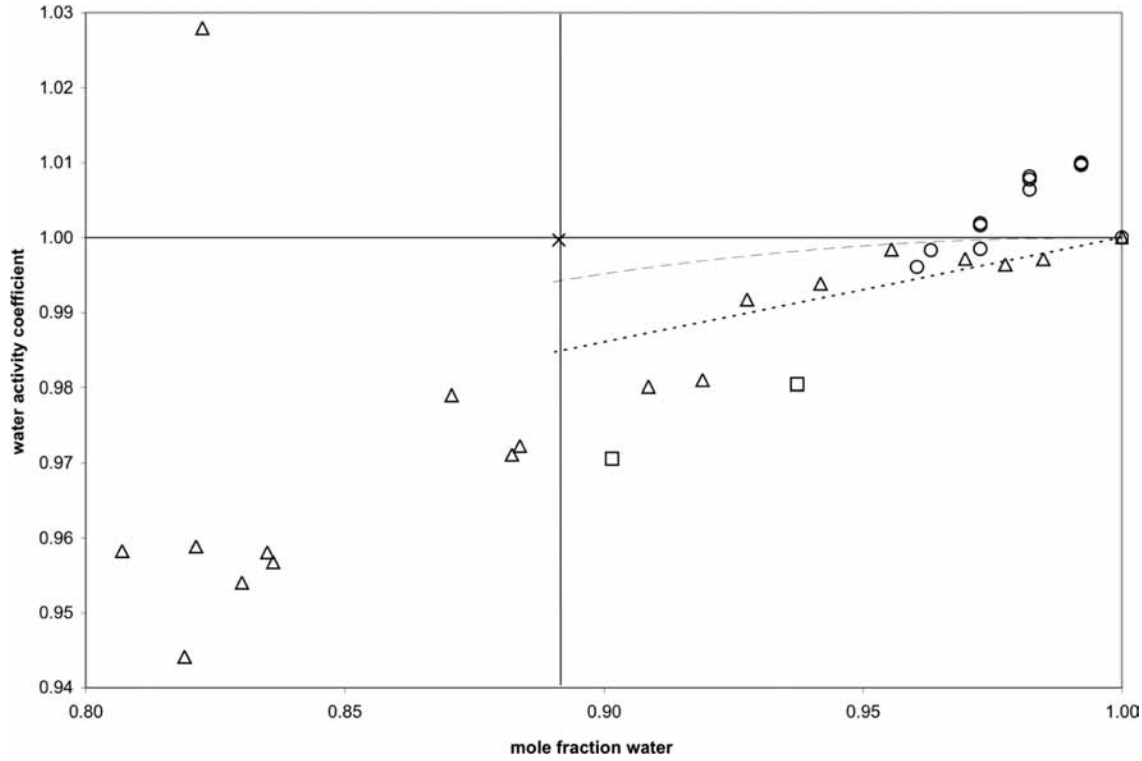

Figure 5. Water activity coefficients for the maleic acid/water system for concentrations under the ice melting envelope (0−21 wt % maleic acid). Symbols used are the following: circles, our DSC data; dotted line, calculated from the van't Hoff factor in Wise et al.;[11] square, Brooks et al.;[10] ex, Marcolli et al.;[12] triangles, Choi and Chan;[9,25] dashed line, calculated from the E-AIM.[13,14] The vertical line at 0.891 mol fraction of water is the deliquescence point at 298.15 K from our experimental data.

an Ar matrix at 7.5 K. The most stable was found to be a structure with all atoms in a plane, and significant hydrogen bonding between the OH group at one end and the C═O at the other. We find qualitative agreement between their spectra for the most stable conformer of maleic acid, our spectra for maleic acid/ice mixtures, and our spectrum of pure, solid maleic acid taken with an ATR accessory. However, the less stable conformers in their study relaxed to the most stable conformer after annealing their samples at 35 K. Thus, it is unlikely our form II maleic acid represents a meta-stable conformer.

Recently Day et al.[24] discovered a second polymorph of maleic acid at ambient temperature and predicted from theoretical calculations the existence of other crystal forms. The new poloymorphic form observed by Day et al. was obtained from a solution made up of 2:1 caffeine:maleic acid in chloroform. When similar crystallization experiments were attempted in methanol, the new polymorph was not observed. Day et al. concluded "the presence of caffeine may have played a structure directing role in the growth of this latent crystal form". It also seems likely there is a solvent effect based on their observations. Therefore, it is possible that water as the solvent in our samples is playing a structure-directing role to a new polymorphic crystal form that is unstable above 247 K. If we assume that all the maleic acid in our DSC samples is undergoing transition from form II to form I at 247 K, then from the measured enthalpies of the transition in our samples, we determined the average energy of this transition is 118 ± 87 J/mol. This energy is the same order of magnitude calculated by Day et al. for the energy difference in the two polymorphs they studied (150 J/mol). On the basis of the experimental and theoretical observations of Day et al., a new polymorphic form of maleic acid that converts to form I at or above 247 K seems to be the most plausible explanation for our form II maleic acid.

Water Activities. In a simple binary system the freezing point depression can be used to determine solvent activities via the equation:

$$\ln a_1 = -\int_{T_f}^{T_f^*} \frac{\Delta H_f}{RT^2}\,\mathrm{d}T \tag{2}$$

where a_1 is the activity of water at T_f, ΔH_f is the molar enthalpy of fusion of ice, $R = 8.314$ J mol^{-1} K^{-1}, T_f is the depressed melting point, and T_f^* is the melting point of pure water. To a first approximation, the enthalpy of fusion can be considered constant as a function of temperature over a small temperature range, and then eq 2 is simply:

$$\ln a_1 = \frac{\Delta H_f}{R}\left(\frac{1}{T_f^*} - \frac{1}{T_f}\right) \tag{3}$$

For the maleic acid/water system, we determined the water activities of our solutions at T_f in the range of the ice melting envelope, $0 < [C_4H_6O_4] < 21$ wt % (representing a temperature range of 273.15 to 268.7 K) using eq 3. From this, water activity coefficients (γ_1) are calculated using $a_1 = \gamma_1 x_1$, with x_1 being the mole fraction of water. These results are plotted in Figure 5 as mole fraction of water versus water activity coefficient (γ_1). Since the activities are calculated at the ice melting point for each concentration, it is not possible for us to differentiate between a concentration and a temperature effect in the water activities of our experiments. Wise et al.[11] determined the van′t Hoff factor for maleic acid/water solutions at 298 K in the concentration range 0−59 wt % maleic acid to be 1.14, where the van′t Hoff equation is given by

$$a_1^{-1} = 1 + i\left(\frac{n_2}{n_1}\right) \tag{4}$$

a_1 is the activity of water, i is the van′t Hoff factor, n_2 is the

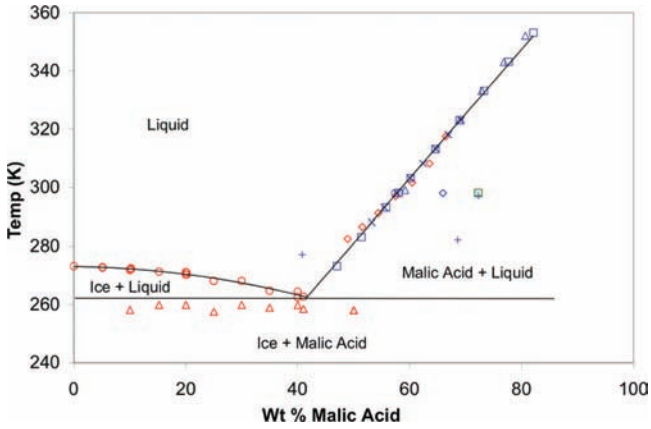

Figure 6. Malic acid/water phase diagram. Red points are our data: circles, ice final melt from DSC data; diamonds, solubility point of malic acid from conductivity data; triangles, eutectic melting from DSC data. Literature data are in blue: triangles, Weiss and Downs;[19] squares, Lange and Sinks;[20] exes, Apelblat and Manzurola;[21] pluses, Brooks et al.;[10] circle, Marcolli et al.;[12] diamond, Wise et al.[11] The green square is the solubility prediction of the E-AIM at 298.15 K.[13,14]

moles of solute, and n_1 is the moles of water. The results of this calculation are given in Figure 5 as a dashed line. Literature values from Brooks et al.[10] at 297 and 277 K (taken at the respective solubility points of maleic acid), Marcolli et al.[12] at 298 K, and the data of Choi and Chan[9,25] at 295.7 K in the range 0.8 to 1.0 water mole fraction are also included. Finally, a fit to data calculated from the extended Aerosol Inorganics Model (E-AIM)[13,14] is included for comparison. Good agreement is seen between our data and the literature data (±1%), including the van′t Hoff predictions of Wise et al. The van′t Hoff prediction reasonably matches the data of Choi and Chan, while the single data point of Marcolli et al. is approximately 2% higher than the data of Choi and Chan and Wise et al. The predictions of E-AIM also follow our data and that of Choi and Chan above about 0.95 mol fraction of water. At lower water concentrations, the deviations between the predictions of E-AIM and the data of Choi and Chan become significant. It should be noted that deliquescence in this system occurs at 0.89 mol fraction of water. Water concentrations below this value represent supersaturated solutions.

dl*-Malic Acid/Water ($C_4H_6O_5/H_2O$).** ***Phase Diagram. We have constructed the solid/liquid phase diagram for the *dl*-malic acid/water system from DSC and conductivity experiments as given in Figure 6, along with solubility data from the literature[10−12,19−21] and the prediction of the E-AIM at 298.15 K.[13,14] The ice melting envelope was determined from DSC experiments; however, the malic acid solid/liquid equilibrium envelope was determined from literature data and our conductivity measurements. The DSC data in this concentration region did not yield clear signals for the dissolution of malic acid into solution, likely because of very weak thermal signals for this process. Also, the eutectic temperatures measured in the DSC experiments appear to be uniformly low. This is also due to the difficulty in accurately determining the onset of eutectic transitions (malic acid dissolving into solution under the ice melting envelope) due to the very small signal for this process. There was significant interference from the very large signal due to ice melting and the closeness in temperature of the eutectic and ice melting envelope. For example, the normalized energy of the eutecitc transition in a 5 wt % malic acid sample was 8.2 J/g compared to the ice melting transition energy of 275.14 J/g. The average eutectic temperature from our DSC data is 259.2 ± 1.0 K. The polynomial coefficients for the fit of the ice and acid liquidus lines using eq 1 are given in Table 1, and the value of the eutectic from this analysis was determined to be 262.58 K at 42.41 wt % malic acid. In our fit for the malic acid liquidus line, we included our conductivity data as well as the solubility data of Lange and Sinks[20] in order to extend the range of malic acid concentrations covered in the parametrization. Given the good agreement between our conductivity measurements and literature values for the malic acid/solution liquidus envelope as well as the clear DSC signals for the ice/liquidus envelope, we recommend the eutectic temperature and composition for this system calculated from the intersection of the two solid/liquid equilibrium envelopes.

Comparing solubility data, we find good agreement between our solubility data for *dl*-malic acid and that from the historical literature[19−21] and the more recent work by Marcolli et al.[12] However, the point measured by Wise et al.[11] for malic acid solubility at 298.15 K is a significantly higher malic acid concentration (65.9 wt %) than given by the historic data (57.7 wt %). While the work of Brooks et al.[10] and results of the E-AIM[13,14] are in good agreement, their solubility points at 297.15 and 298.15 K, respectively, are at even higher malic acid concentrations (72.3 wt % for both). Additionally, the solubility data from Brooks et al. for 282 and 277 K are significantly different from the literature and our data.

Water Activities. For aqueous *dl*-malic acid, the water activities at the temperatures of the ice liquidus line were calculated according to eq 3 in the concentration range 0−40 wt % malic acid from our DSC data (representing the temperature range 273.15 to 264.4 K). These results are plotted in Figure 7 as the mole fraction of water versus water activity coefficient (γ_1). Wise et al.[11] determined the van′t Hoff factor at 298 K for malic acid/water solutions in the concentration range 0−72 wt % malic acid to be 1.87, where the van′t Hoff equation is given by eq 4 above. The results of this calculation are given in Figure 7 as a dotted line. Literature values from Apelblat et al.[26] in the range 288.2 to 323.2 K (taken at the respective solubility points of malic acid), Maffia and Meirelles[27] at 298 K, Peng et al.[25,28] at 298 K, Marcolli et al.[12] at 298 K, and Brooks et al.[10] at 297 and 277 K (taken at the respective solubility points of malic acid) are also included. Finally, the predictions of E-AIM[13,14] are given in the figure as a dashed line. It is seen that our DSC data are in good agreement with that of the literature values over the range of concentrations of our data. The linear relationship found by Wise et al.[11] does not appear to be in agreement with the low concentration malic acid data from multiple groups as given in the figure or the higher concentration data of Peng et al.[28] Also, the point measured by Brooks et al. at 0.915 mol fraction of water appears to be in significant disagreement with the literature data at this composition. It should be noted that this data point was measured at 277 K, which in their experiments they took to be the deliquescence point at 66.0% relative humidity. The error may be in their determination of the solubility of *l*-malic acid at this temperature to be 40.8 wt % malic acid. This is not in agreement with our results and the literature solubility data that predict a saturation concentration of 48.7 wt % malic acid at 277 K with use of eq 1 and our parameters for malic acid as given in Table 1. Finally, the E-AIM predictions at 298.15 K are in good agreement with literature values, though the deliquescence point predicted by the model is at much lower water content than that given by the literature and our data as noted in the phase diagram discussion.

Glutaric Acid/Water. ***Phase Diagram.*** We have constructed the solid/liquid phase diagram for the glutaric acid/water system

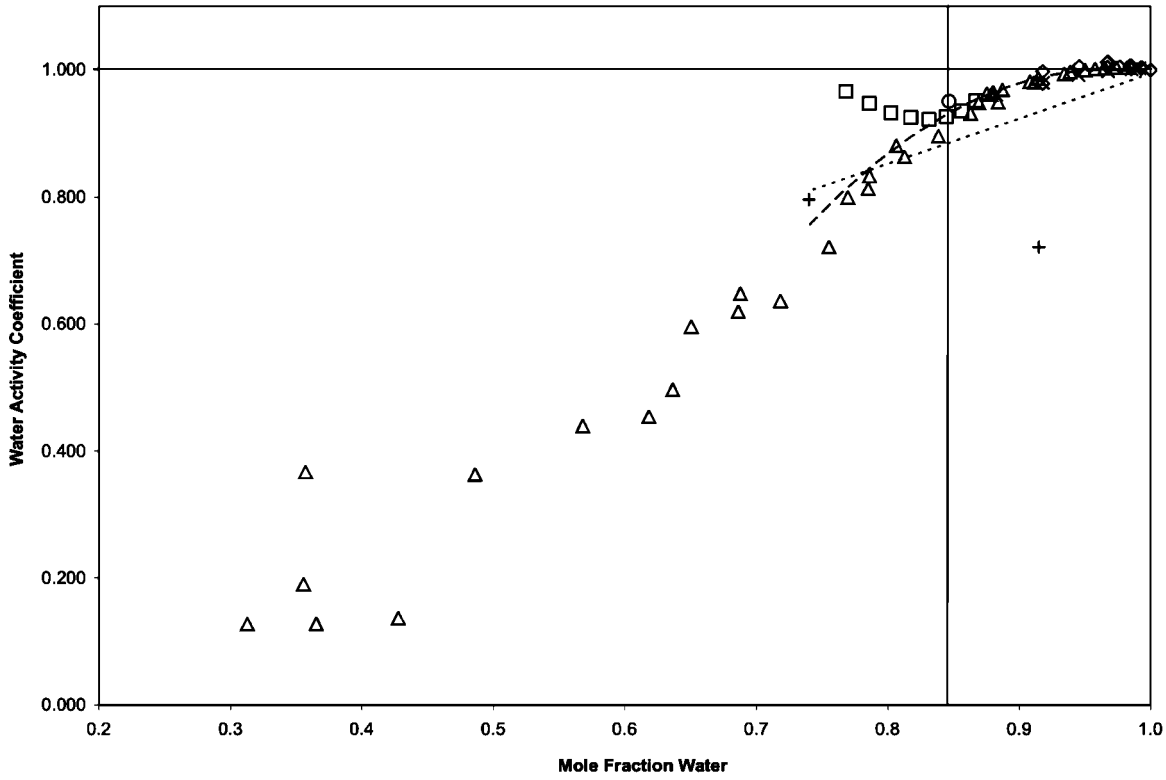

Figure 7. Water activity coefficient as a function of water mole fraction for the malic acid/water system. Symbols used are the following: diamonds, our DSC data; squares, Apelblat et al.;[26] exes, Maffia and Meirelles;[27] triangles, Peng et al.;[25,28] circle, Marcolli et al.;[12] pluses, Brooks et al.[10] The dotted line is calculated with the van′t Hoff factor from Wise et al.;[11] the dashed line is the prediction at 298.15 K of the E-AIM. The vertical line at 0.847 mol fraction of water is the deliquescence point at 298.15 K from solubility[19−21] and our experimental data.

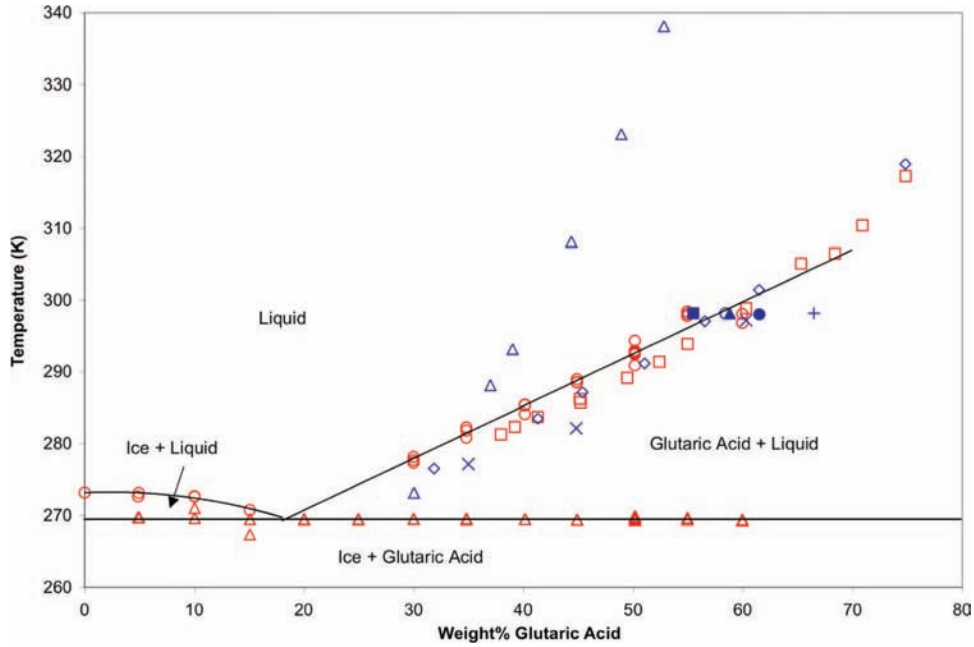

Figure 8. Phase diagram of the glutaric acid/water binary system. Red points are our data: circles, ice final melt or glutaric acid dissolution from DSC data; squares, dissolution of glutaric acid from conductivity data; triangles, eutectic melting from DSC data. Literature data are in blue: solid circle, CRC data;[16] open triangle, Stephen and Stephen Table 1243;[32] open diamond, Stephen and Stephen Table 1244;[31] exes, Brooks et al.;[10] plus, Peng et al.[25,28] solid square, Wise et al.;[11] solid triangle, Marcolli et al.;[12] open circle, prediction of E-AIM at 298.15 K.[13,14]

from DSC and conductivity experiments as given in Figure 8, along with solubility data from the literature,[10,12,16,25,28] and the prediction of the E-AIM at 298.15 K.[13,14] The raw experimental data for this system are included in Table 4S in the Supporting Information. As can be seen in Figure 8, our data are in good agreement with the literature values. The polynomial coefficients for the fit of the ice and acid liquidus lines using eq 1 are given in Table 1. The DSC data for glutaric acid have an average eutectic temperature of 269.59 ± 0.45 K, which is in excellent agreement with the value of 269.51 K at 18.40 wt % glutaric acid calculated from the analysis of the DSC ice melt and acid dissolution curves using eq 1 and the parameters in Table 1. It is noted that our parametrization of the ice liquidus line leads to a prediction of a maximum in the liquidus line temperature

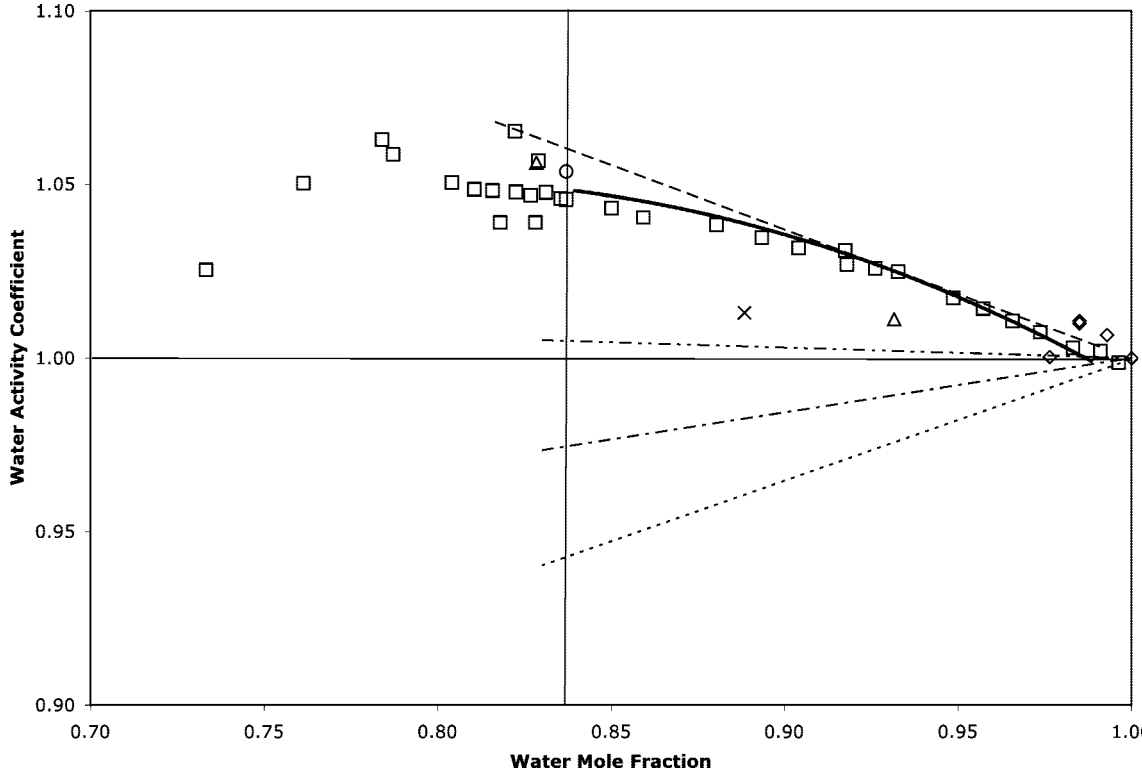

Figure 9. Water activity coefficient as a function of water mole fraction for the glutaric acid/water system. Symbols used are the following: diamonds, our DSC data; squares, Peng et al.;[28] circle, Marcolli et al.;[12] triangles, Brooks et al.;[10] ex, Zardini et al.[33] The dashed line is calculated with the van′t Hoff factor from Wise et al.;[11] dotted, dot-dash, and dot-dot-dash lines are from Koehler et al.[34] for $\nu\Phi$ values of 1.37, 1.16, and 0.97, respectively; the solid curve is the prediction of E-AIM at 298.15 K.[13,14] The vertical line at 0.84 mol fraction water is the deliquescence point at 298.15 K from our experimental data.

of 273.23 K at 2.39 wt % glutaric acid. While this is clearly not physically real, it results from the very shallow eutectic for this system at 18.4 wt %, which results in a very slight slope to the liquidus curve. Combine this with the uncertainty in the experimental data, and the small error in the parametrization of the liquidus line is readily explained. Our measured eutectic temperature is also in good agreement with that of Parsons et al.[29] calculated to be 269.0 K for the glutaric acid/water system. Our conductivity data for the dissolution of glutaric acid is slightly lower in temperature for the same concentration when compared to our DSC data, but is within the experimental uncertainty of our DSC data for nearly all concentrations. The agreement between DSC and conductivity data is better at higher glutaric acid concentrations (>45 wt %).

Comparing to the literature data, there is general agreement with the data from Table 1244 of Stephen and Stephen,[30] which is the data set from Attane and Doumani[31] and our DSC and conductivity data. However, the data from Table 1243 of Stephen and Stephen (Lamouroux[32]) show substantial deviation from our experimental data, and all other data from the literature as seen in the figure. It is unclear why the data of Lamouroux are so inconsistent with other literature data, though there may be confusion over the interpretation of their data. Attane and Doumani interpreted the concentrations of Lamouroux as "grams of acid per 100 cc. of solution", whereas Stephen and Stephen list the concentrations as grams of solute per liter of solvent. We have plotted the latter interpretation as the former requires density data, which are currently unavailable.

There is also good agreement between our data and the single data points of Wise et al.,[11] Lide,[16] Marcolli et al.,[12] and the prediction of E-AIM.[13,14] Poorer agreement is seen with the single data point of Peng et al.[25,28] at 298 K. This may be due to the long time scale of Peng et al.′s experiment to attain full deliquescence of their particle (>12 h), thus increasing the uncertainty in their measurement. Agreement with the solubility measurements of Brooks et al.[10] is good at 297 K, but their data points for 282 and 277 K are lower than our and other literature data.

Water Activities. Water activities for the glutaric acid/water system are shown in Figure 9. Equation 3 was used to determine water activities on the liquidus curve from our DSC data over the concentration range 0 to 15 wt % glutaric acid (representing the temperature range 273.15 to 271 K). In addition, literature data from Peng et al.[25,28] at 298 K, Brooks et al.[10] at 297 and 277 K (taken at the respective solubility points of glutaric acid), Marcolli et al.[12] at 298 K, and Zardini et al.[33] at 291 K are plotted. The water activities calculated for glutaric acid at 298 K from the van′t Hoff factor given in Wise et al.[11] and the predictions of the E-AIM[13,14] are also shown in Figure 9 as a dashed line and a solid curve, respectively. Good agreement is seen for all data sets. It is seen that the predictions of Wise et al. and the E-AIM substantially coincide, and agree well with the data point of Marcolli et al. at 298 K and Brooks et al. at 297 K.

Koehler et al.[34] calculated water activity/concentration relationships at 298 K from their humidified tandem differential mobility analyzer (HTDMA) data using eq 4. However, in their analysis they set $i = \nu\Phi$, where ν is the number of ions each solute molecule dissociates into and Φ is the molal osmotic coefficient. This equality is not strictly true,[35,36] and thus it is not clear that a direct comparison can be made between their mole fraction/activity relationships and those determined by Wise et al.[11] Koehler et al. report three values for $\nu\Phi$, from which three curves of water mole fraction vs activity coefficient

can be calculated. These curves are plotted in Figure 9. It is seen that a value of $\nu\Phi = 1.37$ yields a line that substantially coincides with the data of Peng et al.;[28] however, as mentioned above, these data are not in line with other literature data, including the van′t Hoff factor results of Wise et al., the predictions of E-AIM, or our DSC data. Unfortunately, our DSC data cover a very small concentration range, where the literature data are nearly all in agreement. Thus our data do not help clarify the discrepancies in the literature regarding the concentration/activity relationships for this system.

Succinic Acid/Water ($C_4H_6O_4/H_2O$). ***Phase Diagram.*** Our experimental thermodynamic data for this system are given in Table 4S in the Supporting Information. Thermal signals from the DSC for dissolution of succinic acid were weak, and thus it was difficult to establish points on the liquidus line, especially at higher succinic acid concentrations. Good agreement was found between our DSC and conductivity data points and solubility data from the literature.[10−12,21,30] Succinic acid is fairly insoluble in water, thus resulting in a eutectic point at a very low concentration of succinic acid. Peng et al.[28] have reported that succinic acid is a nondeliquescent species and therefore nonhygroscopic, while Wex et al.[37] and Marcolli et al.[12] measured deliquescence at 99% and 99.1% relative humidity, respectively. Our phase diagram of the succinic acid/water system confirms these high relative humidity deliquescence points. The slight solubility of this acid also leads to the ice melting envelope and eutectic transition temperature being very close. To determine the eutectic composition and temperature, the ice melting and acid dissolution envelope equations were solved simultaneously. A eutectic point of 272.50 K with a composition of 2.08 wt % succinic acid was calculated. An average of the eutectic transition temperatures over the concentration range analyzed on the DSC was 272.71 ± 0.11 K. These values compare well with Parsons′ calculated eutectic point of 273.2 K[29] and the temperature of 272.6 K reported by Zobrist et al.,[38] though they were unable to discern between the eutectic melt and the ice melt.

Water Activities. For the succinic acid/water system, we determined the water activities of our solutions at T_f in the range of the ice melting envelope, $0 < [C_4H_6O_4] < 2.2$ wt % using eq 3. Over this narrow concentration range we determined activity coefficients from our data to be within 0.3% of unity, which is in agreement with measurements by Peng et al.[28] at 298 K. Data from measurements taken with an electronic hygrometer and deionized water by Maffia and Meirelles[27] for water activities of succinic acid at 298.15 K are also within 0.3% of unity over the range 1.5−5.5 wt % succinic acid. Marcolli et al.[12] measured the water activity at 298 K in a saturated succinic acid solution, which gives a water activity coefficient of 1.00. Unfortunately, although Wise et al.[11] studied the succinic acid/water system they did not report a van′t Hoff factor for the water activity due to the low solubility of the acid; however, they did report a single datum at 298 K (8.4 wt % succinic acid) with an activity coefficient within 1% of unity. Finally, Brooks et al.[10] report a single data point at 8.7 wt % succinic acid and 298 K with an activity coefficient of 0.923, or about 8% below unity.

Conclusions

The phase diagrams of maleic acid/water, *dl*-malic acid/water, glutaric acid/water, and succinic acid/water have been studied by using differential scanning calorimetry (DSC) and infrared (IR) spectroscopy of thin films. From these studies the ice melting envelope, eutectic concentration and temperature, parametrization of ice and acid liquidus phase boundaries, and water activities were determined for each aqueous acid system along with comparisons to literature data. In general we find good agreement with literature data for the solubility of the organic acids, and water activities for each system as determined from our DSC data. However, for some of the systems, especially at larger acid concentrations, the van′t Hoff factor predictions of Wise et al.[11] for water activities do not match the experimental determinations of our data or that in the literature. As seen in eq 4, the van′t Hoff factor assumes a constant relationship between the activity of water and the moles of solute, thus a linear relationship between solute concentration and solution nonideality, which is to account for the degree of dissociation of electrolyte solutions. However, with weakly dissociating molecules, such as those studied here, the relationship is not observed to be linear, indicating the level of dissociation changes with concentration. In all of the systems we studied, there is an adherence to ideal behavior at low acid concentrations before nonideal conditions commence at higher acid concentrations. This is seen in the water activity vs activity coefficient plots for maleic, *dl*-malic, and glutaric acids. In the case of succinic, since solubility is so low, the solution acts as ideal up to the room temperature solubility point. Thus in atmospheric models, this nonlinear relationship needs to be taken into account when predicting solution activities and water vapor pressures, as it appears the van′t Hoff equation is insufficient to describe these behaviors. The method described by Prupacher and Klett[35] using molal osmotic coefficients and a parameter for the total number of ions in solution would seem to be more accurate. There were also differences between the predictions of Wise et al., the E-AIM,[13,14] and the experimental data for each system, except succinic. Malic acid/water seemed to pose the most difficulty for the models predicting acid solubility at 298 K.

We also observed an irreversible solid−solid phase transition in the maleic acid/water system. Signatures were seen in both DSC and IR experiments, with an average transition temperature of 246.71 ± 0.96 K, average enthalpy of transition of 118 ± 87 J/mol, and a characteristic IR absorption for the low temperature phase at 1330 cm^{-1}. We conclude that this transition is due to the reordering of a metastable crystal form of maleic acid ("form II", that forms on crystallization of the sample) into the most stable crystal form of maleic acid ("form I", as illustrated by Day et al.[24]) upon warming through the transition temperature. It is unclear whether formation of form II maleic acid in atmospheric aerosols will have an impact on aerosol chemistry as compared to form I maleic acid. Laboratory and/or theoretical studies would need to be performed on each form to determine if surface chemistry is a function of the specific crystal structure of maleic acid.

Acknowledgment. This work was supported by the NSF Atmospheric Chemistry Program (ATM-0442273). We gratefully acknowledge the insightful comments of an anonymous reviewer.

Supporting Information Available: Figure 1S shows typical conductivity data and analysis; Table 1S contains the experimentally determined transition temperatures for the maleic acid/water system used to create Figure 1; Table 2S contains the experimentally determined transition temperatures for the *dl*-malic acid/water system used to create Figure 5; Table 3S contains the experimentally determined transition temperatures for the glutaric acid/water system used to create Figure 8; and Table 4S contains the experimentally determined transition

temperatures for the succinic acid/water system. This material is available free of charge via the Internet at http://pubs.acs.org.

Note Added after ASAP Publication. This article posted ASAP on October 29, 2008. Figure 9 has been revised. Paragraph 14 in the Results section has also been revised due to the new figure. The correct version posted on November 13, 2008.

References and Notes

(1) Kawamura, K.; Ikushima, K. *Environ. Sci. Technol.* **1993**, *27*, 227–2235.

(2) Sheridan, P. J.; Brock, C. A.; Wilson, J. C. *Geophys. Res. Lett.* **1994**, *23*, 2587–2590.

(3) Kawamura, K.; Semere, R.; Imai, Y. *J. Geophys. Res* **1996**, *101*, D13 18721–18728.

(4) Kawamura, K.; Semere, R.; Imai, Y.; Fujii, Y.; Hayashi, M. *J. Geophys. Res.* **1996**, *101*, 18721–18728.

(5) Murphy, D. M.; Thomson, D. S.; Mahoney, M. J. *Science* **1998**, *282*, 1664–1669.

(6) Loflund, M.; Kaser-Giebl, A.; Schuster, B.; Giebl, H.; Hitzenberger, R.; Puxbaum, H. *Atmos. Environ.* **2002**, *36*, 1553–1558.

(7) Tervahattu, H.; Hartonen, K.; Kerminen, V.; Kupiainen, K.; Aarnio, P.; Koskentalo, T.; Tuck, A. F.; Vaida, V. *J. Geophys. Res.* **2002**, *107*, D7 AAC-1.

(8) Saxena, P.; Hildemann, L. M.; McMurry, P. H.; Seinfeld, J. H. *J. Geophys. Res.* **1995**, *100*, 18755–18700.

(9) Choi, M. Y.; Chan, C. K. *J. Phys. Chem. A* **2002**, *106*, 4566–4572.

(10) Brooks, S. D.; Wise, M. E.; Cushing, M.; Tolbert, M. A. *Geophys. Res. Lett.* **2002**, *29*, 1917.

(11) Wise, M. A.; Surratt, J. D.; Curtis, D., B.; Shilling, J. E.; Tolbert, M., A. *J. Geophys. Res.* **2003**, *108*, D20 4638.

(12) Marcolli, C.; Luo, B.; Peter, T. *J. Phys. Chem. A* **2004**, *108*, 2216–2224.

(13) Clegg, S. L.; Seinfeld, J. H. *J. Phys. Chem. A* **2006**, *110*, 5692−5717 (web version: www.aim.env.uea.ac.uk/aim/aim.php).

(14) Clegg, S. L.; Seinfeld, J. H. *J. Phys. Chem. A* **2006**, *110*, 5718−5734 (web version: www.aim.env.uea.ac.uk/aim/aim.php).

(15) Zhang, R.; Wooldridge, P. J.; Abbatt, J. P. D.; Molina, M. J. *J. Phys. Chem.* **1993**, *97*, 7351–7358.

(16) Lide, D. R., Ed. *CRC Handbook of Chemistry and Physics*, 74th ed.; CRC Press: Boca Raton, FL, 1993; 3-208,351. and 6-58.

(17) Miller, F. A.; Wilkins, C. H. *Anal. Chem.* **1952**, *24*, 1253–1294.

(18) Wendlandt, W. W. *Thermal Analysis*; John Wiley: New York, 1986.

(19) Weiss, J. M.; Downs, C. R. *J. Am. Chem. Soc.* **1923**, *45*, 1003–1008. Also found in: Timmermans, J. *The Physico-Chemical Constants of Binary Systems in Concentrated Solutions*; Interscience: New York, 1960; Vol. 4.

(20) Lange, N. A.; Sinks, M. H. *J. Am. Chem. Soc.* **1930**, *52*, 2602–2604. Also found in: Stephen,H.; Stephen, T. *Solubilities of Inorganic and Organic Compounds*; MacMillan: New York, 1963; Vol. *1*.

(21) Apelblat, A.; Manzurola, E. *J. Chem. Thermodyn.* **1987**, *19*, 317–320.

(22) Brooks, S. D.; Garland, R M.; Wise, M. E.; Prenni, A. J.; Cushing, M.; Hewitt, E.; Tolbert, M. A. *J. Geophys. Res* **2003**, *108*, D15 4487.

(23) Macoas, E. M. S.; Fausto, R.; Lundell, J.; Petterson, M.; Khriachtchev, L.; Rasanen, M. *J. Phys. Chem. A* **2001**, *105*, 3922–3933.

(24) Day, G. M.; Trask, A. V.; Motherwell, W. D. S.; Jones, W. *Chem. Commun.* **2006**, 54–56.

(25) Raw data in excel files for the systems studied by Dr. Chak K. Chan′s group were accessed at: http://ihome.ust.hk/∼keckchan/hygroscopic.html.

(26) Apelblat, A.; Dov, M.; Wisniak, J.; Zabicky, J. *J. Chem. Thermodyn.* **1995**, *27*, 35–41.

(27) Maffia, M. C.; Meirelles, J. A. *J. Chem. Eng. Data* **2001**, *46*, 582–587.

(28) Peng, C.; Chan, M. N.; Chan, C. K. *Environ. Sci. Technol.* **2001**, *35*, 4495–4501.

(29) Parsons, M. T.; Mak, J.; Lipetz, S. R.; Bertram, A. K. *J. Geophys. Res.* **2004**, *109*, D06216.

(30) Stephen, H.; Stephen, T. *Solubilities of Inorganic and Organic Compounds*; MacMillan: New York, 1963; Vol. 1.

(31) Attane, E. C.; Doumani, T. F. *Ind. Eng. Chem.* **1949**, *41*, 2015–2017.

(32) Lamouroux, F. *Compt. Rend.* **1899**, *128*, 998.

(33) Zardini, A. A.; Sjogren, S.; Marcolli, C.; Krieger, U. K.; Gysel, M.; Weingartner, E.; Baltensperger, U.; Peter, T. *Atmos. Chem. Phys. Discuss.* **2008**, *8*, 5235–5268.

(34) Koehler, K. A.; Kreidenweis, S. M.; DeMott, P. J.; Prenni, A. J.; Carrico, C. M.; Ervens, B.; Feingold, G. *Atmos. Chem. Phys.* **2006**, *6*, 795–809.

(35) Pruppacher, H. R.; Klett, J. D. *Microphysics of Clouds and Precipitation*, D. Reidel: Boston, MA, 1980.

(36) Kreidenweis, S. M.; Koehler, K.; DeMott, P. J.; Prenni, A. J.; Carrico, C.; Ervens, B. *Atmos. Chem. Phys.* **2005**, *5*, 1357–1370.

(37) Wex, H.; Ziese, M.; Kiselev, A.; Henning, S.; Stratmann, F. *Geophys. Res. Lett.* **2007**, *34*, L1 7810.

(38) Zobrist, B.; Marcolli, C.; Koop, T.; Luo, B. P.; Murphy, D. M.; Lohmann, U.; Zardini, A. A.; Krieger, U. K.; Corti, T.; Cziczo, D. J.; Fueglistaler, S.; Hudson, P. K.; Thomson, D. S.; Peter, T. *Atmos. Chem. Phys.* **2006**, *6*, 3115–3129.

JP805985T